IOP Concise Physics

Classical Theory of Free-Electron Lasers

A text for students and researchers

Eric B Szarmes

Chapter 11

Laser saturation and output power

11.1 The nature of FEL saturation

The essential richness of FEL physics—the complex, even chaotic, phase space evolution; frequency pulling effects; synchrotron oscillations and sideband formation; the high FEL efficiency; and not least, the MW-level optical micropulse powers delivered at GHz repetition rates—occurs at saturation.

To get at the nature of FEL saturation, examine the (ξ', ν') phase space trajectories for various magnitudes of optical field a', as shown in figure 11.1. These figures were calculated for $\tau = 0 \rightarrow 1$ by straightforward numerical integration of the coupled equations of motion, (9.52) and (9.53); the simulations used $j_F = 1$, but the trajectories are qualitatively independent of j_F.

In all the panels of figure 11.1, the electrons enter the undulator with fixed energy. The optical wave, which typically turns on from weak spontaneous radiation, evolves coherently with an optical frequency corresponding to the peak of the gain curve, with an initial phase velocity of $\nu_0' = 2.606$ for the electrons. This initial phase velocity remains basically fixed at the start of each pass as the coherent optical wave circulates within the resonator. The magnitude of the optical field determines the height of the separatrices, equal to $\Delta\nu' = \pm 2\sqrt{|a|}$ (see (9.6)). Saturation occurs when the separatrices, which initially have a height much smaller than ν_0', grow so large that they capture the electrons in closed phase space orbits.

Initially, in the small signal regime with $|a'|^2 \ll 1$, the electrons evolve in open orbits; the average energy loss of the electrons is small, but the fractional growth of the optical energy on a single pass, $\Delta|a'|^2/|a'|^2$, is large. As the optical field grows to the intermediate regime, $2\sqrt{|a'|} \sim \nu_0'$, some of the electrons become trapped in the phase space buckets enclosed by the separatrices; this represents the transition between the small signal and large signal regimes. In the large signal regime with $|a'|^2 \gg 1$, essentially all of the electrons are trapped in closed orbits within the phase space buckets. In these closed orbits, the electrons do not lose energy indefinitely; instead, they fall only as far as the bottom of the buckets before coming up again and

doi:10.1088/978-1-6270-5573-4ch11

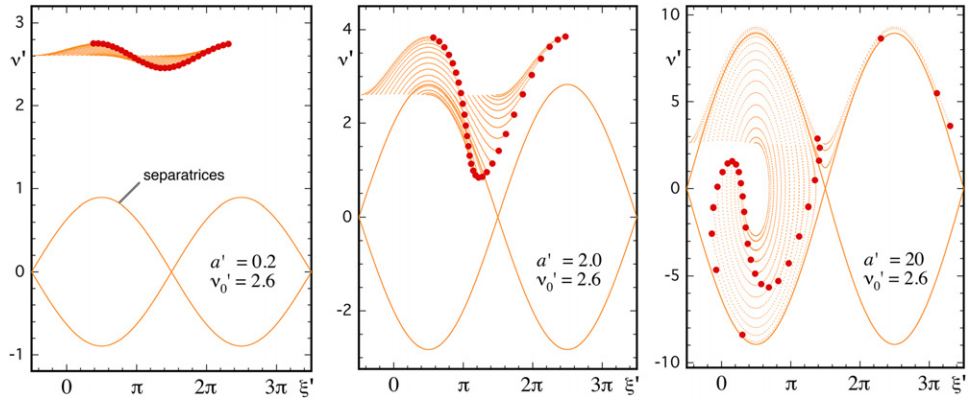

Figure 11.1. The nature of FEL saturation. Left: open orbits, high gain; $|a'|^2$ small, $\frac{\Delta|a'|^2}{|a'|^2}$ large. Center: intermediate regime, onset of particle trapping. Right: closed orbits, saturation; $|a'|^2$ large, $\frac{\Delta|a'|^2}{|a'|^2}$ small.

taking energy from the optical wave. This is the FEL saturation mechanism. In this regime, the energy loss of the electrons is large, but the fractional growth of the optical power, $\Delta|a'|^2/|a'|^2$, is small and continues to decrease with increasing $|a'|^2$. The optical field continues to grow until $\Delta|a'|^2/|a'|^2$ on a single pass decreases to a value equal to the fractional cavity loss. The laser then reaches a type of quasi-stable equilibrium, except for dynamic effects and the possible onset of instabilities discussed below.

11.2 Strong-saturation effects

Frequency pulling. In contrast to lasers based on atomic media, the peak of the FEL gain curve is not centered on the spontaneous spectrum. This has important implications for the evolution of the optical frequency in an FEL. If we compute the gain curves at various levels of saturation by self-consistent integration of the coupled Maxwell–Lorentz equations of motion, we find that in addition to the reduction in gain noted in the preceding section, there is a distortion of the gain curve that pulls peak the of the curve to higher values of $\nu_0'^{\text{opt}}$. This effect is illustrated in figure 11.2, generated for a small-gain current of $j_F = 0.1$.

Since the injected electron energy is typically held fixed, this increase in the peak value of ν_0' causes the optical frequency to be pulled to lower frequencies and longer wavelengths. Indeed, recall that the phase velocity defined in (6.8), $\nu = L_w[(k + k_w)\bar{\beta}_z - k]$, is an implicit function of both γ and ω, i.e. $\nu = \nu(\bar{\beta}_z(\gamma), k(\omega))$. We therefore have

$$\mathrm{d}\nu = \frac{\partial \nu}{\partial \gamma}\mathrm{d}\gamma + \frac{\partial \nu}{\partial \omega}\mathrm{d}\omega \tag{11.1}$$

$$= \frac{\partial \nu}{\partial \bar{\beta}_z}\frac{\mathrm{d}\bar{\beta}_z}{\mathrm{d}\gamma}\mathrm{d}\gamma + \frac{\partial \nu}{\partial k}\frac{\mathrm{d}k}{\mathrm{d}\omega}\mathrm{d}\omega \tag{11.2}$$

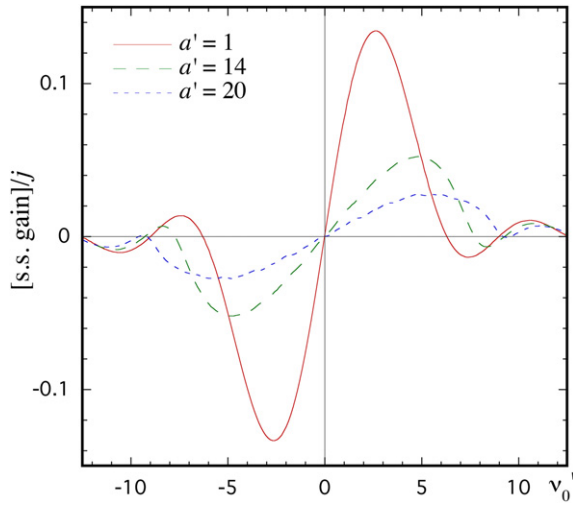

Figure 11.2. Distortion of the FEL gain function for increasing fields ($j_F = 0.1$).

$$\mathrm{d}\nu = L_w k \frac{2k_w}{\gamma k}\mathrm{d}\gamma + L_w\left(\bar{\beta}_z - 1\right)\frac{1}{c}\mathrm{d}\omega \tag{11.3}$$

$$= 4\pi N_w \frac{\mathrm{d}\gamma}{\gamma} - 2\pi N_w \frac{\mathrm{d}\omega}{\omega}, \tag{11.4}$$

where we dropped $k_w \ll k$ in the expression for $\partial\nu/\partial\bar{\beta}_z$ and used the expression for $\mathrm{d}\bar{\beta}_z/\mathrm{d}\gamma$ from (6.14) in the third line, and inserted the slippage condition $1 - \bar{\beta}_z = \lambda/\lambda_w$ from (1.5) in the fourth line. In the evolution of an optical pulse of finite spectral width, whose initial wavelength is established via coherent evolution at the peak of the gain curve in the small-signal regime, the spectral content is slowly replaced in the large-signal regime by longer wavelengths due to the shift in $\nu_0'^{\mathrm{opt}}$. This process occurs over many passes in the resonator as the old radiation decays away and is replaced by optical growth at the new wavelengths.

Frequency pulling is associated with the phase space behavior of the electrons at saturation, as we see in figure 11.3. In the presence of large optical fields, the phase space bucket height grows much higher than the initial phase velocity of $\nu_0'^{\mathrm{opt}} = 2.606$. For separatrices corresponding to lower optical frequencies (larger values of ν_0'), the electrons have more room at the top of the buckets to fall a greater distance in $\Delta\nu'$ even as they remain trapped, yielding a greater energy loss and increased optical gain. The optical wave is thus pulled to lower frequencies and longer wavelengths over many passes in the resonator.

Synchrotron oscillations and sideband instability. In strong optical fields, the electrons can execute many closed orbit revolutions in a single pass through the undulator. These phase space revolutions are called *synchrotron oscillations* and the corresponding frequency is the *synchrotron frequency*. The revolutions are well

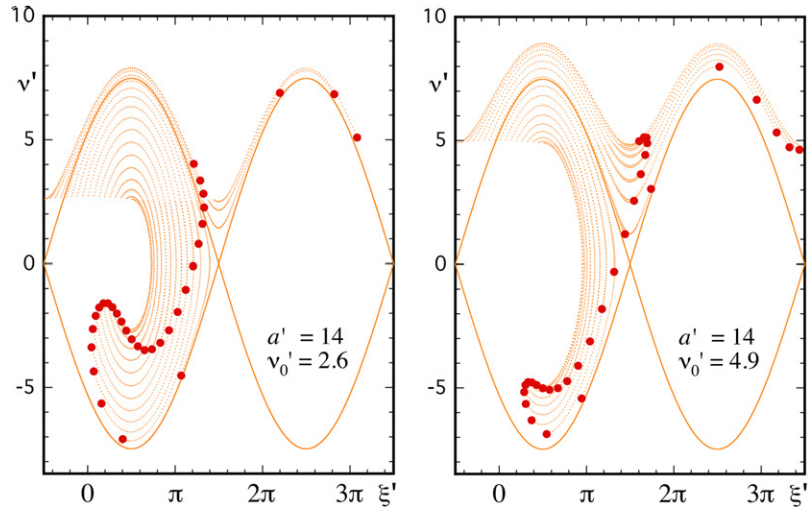

Figure 11.3. The phase space origin of the frequency pulling effect.

represented by the electrons near the stable points in phase space. From the pendulum equation, (9.53), with $\phi' = 0$, we have

$$\frac{\mathrm{d}^2\xi'}{\mathrm{d}\tau^2} = |a'|\cos\xi' = -|a'|\sin(\xi' - \xi'_s) = -|a'|\sin\Delta\xi'; \quad \xi'_s = \frac{\pi}{2} \tag{11.5}$$

$$\text{so} \quad \frac{\mathrm{d}^2(\xi' - \xi'_s)}{\mathrm{d}\tau^2} = \frac{\mathrm{d}^2\Delta\xi'}{\mathrm{d}\tau^2} = -|a'|\sin\Delta\xi' \simeq -|a'|\Delta\xi'; \quad \Delta\xi' \ll 1. \tag{11.6}$$

The electron phase thus oscillates as $\Delta\xi' = \Delta\xi'_0\cos[\sqrt{|a'|}\,\tau]$ and the number of synchrotron oscillations in a single pass through the undulator ($\tau = 1$) equals $\sqrt{|a'|}/2\pi$. Electrons are forced to the bottom of the buckets ($\sqrt{|a'|} = \pi$) for $|a'| = \pi^2 \simeq 10$ and execute a single phase space revolution for $|a'| = 4\pi^2 \simeq 40$.

Synchrotron oscillations, when coupled with optical slippage, lead to an interesting phenomenon called the *sideband instability*. Consider two adjacent sections of an optical wave intense enough to drive one complete synchrotron oscillation, each section roughly one half of a slippage length long ($N_w\lambda/2$). Let the leading one of these sections be coincident with a given group of electrons on their downward swing at the start of the undulator; this section of the wave will be preferentially amplified due to large energy extraction from the electrons. However, by the time these electrons swing back up, they will be coincident with the trailing section of the optical wave because of slippage. This section of the wave will be attenuated due to the loss of optical energy to the coincident electrons.

Thus, the optical wave develops *spiking* in the time domain, a chaotic behavior known as the sideband instability. Its onset generally requires optical fields large enough to force at least one phase space revolution in a single pass through the

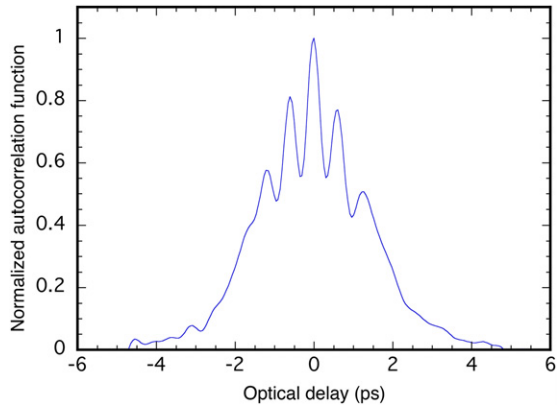

Figure 11.4. Measured autocorrelation function on the Mark III FEL at 3.2 μm showing optical spiking.

undulator, with adjacent spikes roughly separated by the slippage length $N_w\lambda$. An actual measurement of spiking is shown in figure 11.4.

The name 'sideband instability' derives from the associated perturbation in the optical spectrum. Spiking is clearly an amplitude modulation effect driven by the vertical motion of the electrons in phase space. But the accompanying horizontal motion of the electrons in their phase space orbits drives the phase of the optical wave and leads to phase modulation. One of the AM sidebands is evidently canceled by the coincident PM sideband, and the result is a single sideband on the low frequency side of the optical spectrum. Although the sideband instability leads to increased energy extraction, sideband growth is intrinsically chaotic, with sidebands eventually acquiring their own sidebands, and so on. Such spectral broadening and chaotic spiking are often undesirable for research applications using short pulses.

As noted above, the sideband instability turns on when the optical field is sufficiently large to drive at least one synchrotron oscillation, which is often the case when the fractional cavity loss of the optical resonator is sufficiently small. However, the development of spiking on multiple passes in the resonator also requires that the downward motion of the electrons in phase space at a given time τ remain successively coincident with the corresponding spike in the co-propagating optical wave at the same time τ. This is possible only if the resonator is set near its synchronous length (see section 10.4). A small degree of cavity detuning is often sufficient to extinguish the growth of the sideband instability.

11.3 Intensity dependence

In the regime of long electron bunches and laser pulses (with slippage parameter $\mu_c \lesssim 0.2$ or so), a useful and quite universal analysis of FEL saturation can be developed. In this regime, we assume that the laser spectrum is sufficiently narrow that the dynamic distortion of the gain curve at saturation does not have sufficient time to appreciably pull the optical frequency from its small-signal value within the finite duration of the macropulse. We also neglect the formation of sidebands, which assumption is justified independently. These constraints allow us to neglect all

microtemporal perturbations and to base our analysis on the CW equations of motion. Short-pulse supermode effects are omitted, because laser lethargy and electron beam dispersion are negligible at saturation, as explained in section 10.5. Finally, to develop a basic quantitative understanding of saturation, we initially neglect energy spread, to be included in section 11.6.

The analytical procedure employs a straightforward numerical integration of the coupled Maxwell–Lorentz equations of motion over a single pass in the undulator, for different CW optical fields a_0' and current densities j_F, at the peak of the FEL gain curve, $\nu_0'^{\text{opt}} \simeq 2.606 - 0.022 j_F + 0.00016 j_F^2$ (see text following (10.15)). For this analysis we employ the coupled equations derived in section 9.3, (9.52) and (9.53),

$$\frac{\mathrm{d}a'}{\mathrm{d}\tau} = -j_F \langle \mathrm{e}^{-\mathrm{i}\xi'} \rangle_{\xi_0'} \tag{11.7}$$

$$\frac{\mathrm{d}\nu'}{\mathrm{d}\tau} = |a'| \cos(\xi' + \phi'), \tag{11.8}$$

where $j_F = \langle j_L |f_p|^2 R_F \rangle$ and $|a'|^2 = |a_p|^2 \langle R_F^2 |f_p|^2 \rangle$. Energy conservation, (9.49), is written

$$-2 j_F \langle \Delta\nu \rangle_{\xi 0} = \Delta |a'|^2 \qquad \text{or} \qquad -2 \frac{j_L}{R_F} \langle \Delta\nu \rangle_{\xi_0} = \Delta |a_p|^2. \tag{11.9}$$

where $\Delta\nu' = \Delta\nu$. Upon solving (11.7) and (11.8) numerically at peak $\nu_0'^{\text{opt}}$, we can approximate the results by the following expression:

$$G_{\text{sat}} \equiv \frac{\Delta |a'|^2}{|a'|^2} = \frac{G'(j_F)}{\left[1 + \left(\dfrac{|a'|}{4\pi}\right)^2\right]^{\sqrt{\pi}}}, \tag{11.10}$$

where $G'(j_F)$ is given in (10.15). The coefficients '4π' and '$\sqrt{\pi}$' are *mnemonic*; numerically, we find

$$\text{`}4\pi\text{'} = 13.60 - 0.257\, j_F + 0.00942\, j_F^2 - 0.000150\, j_F^3 \tag{11.11}$$

$$\text{`}\sqrt{\pi}\text{'} = 1.800 - 0.0114\, j_F + 0.000864\, j_F^2 - 0.0000159\, j_F^3. \tag{11.12}$$

For $j_F \leqslant 22$ these expressions convey an accuracy of $|\Delta G_{\text{sat}}|/G_{\text{sat}} < 3.5\%(7\%)$ for $|a'| \leqslant 19(30)$. Nevertheless, considerable accuracy is retained in analyses using the mnemonic values 4π and $\sqrt{\pi}$. We see that the intensity dependence of FEL saturation, obtained here by rigorous numerical integration of the equations of motion, manifestly does not correspond to the saturation mechanism of homogeneously broadened atomic lasers, $G \sim [1 + I/I_{\text{sat}}]^{-1}$. This has important implications for the analysis of optical resonators, as we discuss below.

11.4 Analysis of optical resonators

Consider a generic FEL optical resonator with fractional cavity loss δ_c and output coupling δ_{oc}, illustrated in figure 11.5. In the small signal regime, the net gain in a single round trip is

$$1 + G_{net} = (1 + G_{ss})(1 - \delta_c) > 1, \tag{11.13}$$

where G_{ss} is the small-signal, single-pass laser gain; see section 10.5.

For steady state oscillation at saturation, we have

$$1 = (1 + G_{sat})(1 - \delta_c); \qquad 1 + G_{sat} = \frac{1}{1 - \delta_c}; \qquad G_{sat} = \frac{\delta_c}{1 - \delta_c}. \tag{11.14}$$

The output power is thus proportional to

$$|a'|^2_{out} = |a'|^2(1 + G_{sat})\delta_{oc} \tag{11.15}$$

$$= |a'|^2 \frac{\delta_c}{1 - \delta_c}\left(\frac{\delta_{oc}}{\delta_c}\right) \tag{11.16}$$

$$= |a'|^2 G_{sat}\eta_{oc}; \tag{11.17}$$

$$\text{or} \quad |a'|^2_{out} = |a'|^2 \eta_{oc} \frac{G'}{\left[1 + \left(\frac{|a'|}{4\pi}\right)^2\right]^{\sqrt{\pi}}}, \tag{11.18}$$

where we define the *output coupling efficiency* $\eta_{oc} \equiv \frac{\delta_{oc}}{\delta_c}$ as the fraction of total cavity loss that appears as usable output coupling. This parameter is typically known by design. From the known cavity losses δ_c we can calculate the steady-state saturated gain G_{sat} from (11.14), then calculate $|a'|^2$ at saturation from (11.10) and finally calculate $|a'|^2_{out}$ from (11.17).

Optimum output coupling. What is the optimum cavity loss δ_c for a known value of the small-signal gain G'? Physically, we might expect there to be some optimum value: if δ_c is too large then no power builds up, and if δ_c goes to zero (including δ_{oc}!) then no power gets out.

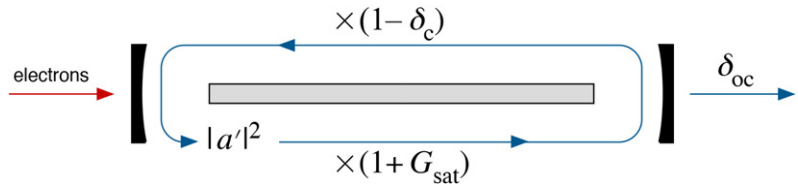

Figure 11.5. Fractional gain and loss factors in an optical resonator.

Since equation (11.18) gives $|a'|^2_{\text{out}}$ as a function of $|a'|^2$, we can maximize $|a'|^2_{\text{out}}$ versus $|a'|^2$ by differentiation. Using mnemonic values for the coefficients, the result is

$$|a'|^2 = |a'|^2_{\text{opt}} = \frac{(4\pi)^2}{\sqrt{\pi} - 1} \quad \rightarrow \quad |a'|_{\text{opt}} = 14.3. \tag{11.19}$$

This value of the optimum intracavity power is completely independent of the design of the optical resonator! For this value of $|a'|_{\text{opt}}$, the electrons undergo 0.6 phase space revolutions (see figure 11.3), so the assumption that sidebands do not turn on is a sensible one. It is perhaps not surprising that optimum energy extraction should correspond to electrons that have descended to the bottom of the phase space buckets. The associated saturated gain is

$$G_{\text{sat}} = \frac{G'}{\left[1 + \dfrac{1}{\sqrt{\pi} - 1}\right]^{\sqrt{\pi}}} = \frac{G'}{4.36}, \tag{11.20}$$

and the optimum cavity losses from (11.14) are

$$\delta_c^{\text{opt}} = \frac{G_{\text{sat}}}{1 + G_{\text{sat}}} = \frac{G'}{4.36 + G'}. \tag{11.21}$$

Finally, the optimum output power from (11.17) is proportional to

$$|a'|^2_{\text{out}} = |a'|^2_{\text{opt}} G_{\text{sat}} \eta_{\text{oc}} = 46.9\, G' \eta_{\text{oc}}. \tag{11.22}$$

Of course, greater accuracy is obtained in this analysis using the previous expansions for the coefficients '4π' and '$\sqrt{\pi}$' from (11.11) and (11.12).

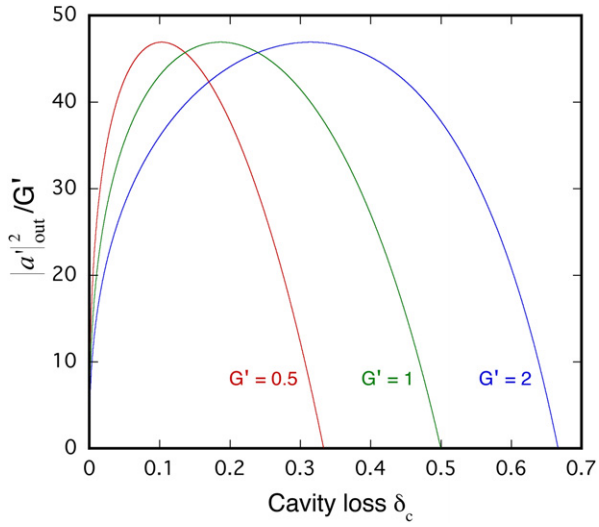

Figure 11.6. Outcoupled optical power as a function of cavity loss.

These results exemplify a fundamental difference in the saturation mechanism in FELs as opposed to conventional lasers, which distinction can be traced back to the appearance of the exponent $\sqrt{\pi}$ in the denominator of (11.10): in conventional lasers, the corresponding exponent does not exceed unity and it is not possible to optimize the total cavity loss δ_c. Instead, it is only possible to optimize the out-coupled cavity loss δ_{oc} for a specified value of the non-outcoupled cavity loss δ_{fixed}, where $\delta_c = \delta_{oc} + \delta_{fixed}$.

Optical power. The conversion of optical power between $|a'|^2$ and $|a_p|^2$ was calculated in (10.13),

$$|a'|^2 = 2q_E|a_p|^2, \tag{11.23}$$

where q_E is defined in (10.11). The optical power in the TEM_{00} mode (with the subscript indicating *optical*) is

$$P_{op} = \iint \mathrm{d}x\,\mathrm{d}y\,\frac{c}{4\pi}|\hat{E}|^2 \tag{11.24}$$

$$= \frac{c}{4\pi}\pi w_0^2 \iint \frac{\mathrm{d}x\,\mathrm{d}y}{\pi w_0^2}|c_p|^2 u_p^* u_p \tag{11.25}$$

$$= \frac{c}{4\pi}\pi w_0^2\,|c_p|^2; \tag{11.26}$$

$$\text{or}\quad P_{op}[\text{watts}] = 10^{-7}\left[\frac{\text{joules}}{\text{erg}}\right]\times\frac{\gamma^4 m^2 c^5}{32\,\pi^3 e^2 N_w^4 \lambda_w^2 \hat{K}_f^2}\cdot\frac{\pi w_0^2}{2}\,|a_p|^2, \tag{11.27}$$

where all physical quantities on the rhs are in CGS units and we converted from c_p to a_p using (8.14).

If we calculate $|a'|^2_{out}$ as a function of δ_c (with $\eta_{oc} = 1$), we find that the factor of '46.9' in (11.22) varies as

$$\frac{|a'|^2_{out}}{G'} = (4\pi)^2\left(\left[\frac{G'(1-\delta_c)}{\delta_c}\right]^{1/\sqrt{\pi}} - 1\right)\frac{\delta_c}{G'(1-\delta_c)}. \tag{11.28}$$

These curves are shown in figure 11.6 for $G' = 0.5;\ 1;\ 2$, and are quite broad; the range of δ_c for which $|a'|^2_{out}$ exceeds 90% of its maximum value is on the order of δ_c itself. Thus, the *net* round-trip, small-signal gain can be substantially increased by decreasing the cavity loss δ_c at little expense to the outcoupled power at saturation.

Example. What are the optimum cavity losses and output power for the example in section 10.5? Use both the mnemonic values of 4π and $\sqrt{\pi}$ and their numerical expansions. Assume $q_\gamma = 1$ and $\eta_{oc} = 1$.

Solution. In that example we calculated $j_F = 7.792$, for which

$$G'(j_F) = 1.355 \tag{11.29}$$

from (10.15). Using mnemonic results from (11.21) and (11.22), we find $\delta_c^{\text{opt}} = 23.7\%$ and $|a'|^2_{\text{out}} = 63.5$. With the previous value of $q_E = 0.700$ we have

$$|a_p|^2_{\text{out}} = \frac{|a'|^2_{\text{out}}}{2q_E} = 45.4. \tag{11.30}$$

Substituting this value for $|a_p|^2_{\text{out}}$ into (11.27), together with the parameters listed in the original example in section 9.1, yields an outcoupled power of $P_{\text{out}} = 8.81$ MW.

If we now use the full expansions for '4π' and '$\sqrt{\pi}$' from (11.11) and (11.12), we calculate '4π' = 12.10 and '$\sqrt{\pi}$' = 1.756. From (11.19) we have

$$|a'|^2 = |a'|^2_{\text{opt}} = \frac{(4\pi)^2}{\sqrt{\pi} - 1} = \frac{(12.10)^2}{1.756 - 1} \quad \rightarrow \quad |a'|_{\text{opt}} = 13.92, \tag{11.31}$$

and the corresponding saturated gain from (11.20) is

$$G_{\text{sat}} = \frac{G'}{\left[1 + \dfrac{1}{\sqrt{\pi} - 1}\right]^{\sqrt{\pi}}} = \frac{G'}{\left[1 + \dfrac{1}{1.756 - 1}\right]^{1.756}} = \frac{G'}{4.39}. \tag{11.32}$$

The optimum cavity losses and output power from (11.14) and (11.17) are then

$$\delta_c^{\text{opt}} = \frac{G_{\text{sat}}}{1 + G_{\text{sat}}} = \frac{G'}{4.39 + G'} = 23.6\%, \tag{11.33}$$

$$|a'|^2_{\text{out}} = |a'|^2_{\text{opt}} G_{\text{sat}} = 44.1\ G' = 59.8. \tag{11.34}$$

The resulting output power is $P_{\text{out}} = 8.3$ MW. Measured outcoupled optical powers from the Mark III FEL are actually of this magnitude—divided into four separate pulses, one from each surface of the intracavity Brewster plate output coupler.

11.5 Extraction efficiency

Into the second of (11.9) for energy conservation,

$$-2\frac{j_L}{R_F}\langle \Delta\nu \rangle_{\xi_0} = \Delta|a_p|^2, \tag{11.35}$$

substitute the expressions for $\Delta\nu$, j_L, R_F and $\Delta|a_p|^2$ in CGS units from (7.36, 8.15, 8.32, 8.38, 11.27):

$$\begin{aligned} -2 \cdot \frac{8\pi^2 e^2 N_w^3 \lambda_w^2 \hat{K}_f^2}{\gamma^3 mc^2} \frac{(I/e)_{\text{MKS}}}{c\ A_e} \cdot \frac{A_e}{\pi w_0^2} \cdot 4\pi N_w \left\langle \frac{\Delta\gamma}{\gamma} \right\rangle \\ = \Delta P_{\text{op}} \cdot \frac{2}{\pi w_0^2} \cdot \frac{32\ \pi^3 e^2 N_w^4 \lambda_w^2 \hat{K}_f^2}{\gamma^4\ m^2 c^5}. \end{aligned} \tag{11.36}$$

This simplifies to

$$\Delta P_{\text{op}} = (I/e)_{\text{MKS}} \langle \Delta(\gamma mc^2) \rangle \tag{11.37}$$

$$\Delta P_{\text{op}} = I_{\text{MKS}} \frac{\gamma mc^2}{e_{\text{MKS}}} \left\langle \frac{\Delta\gamma}{\gamma} \right\rangle \tag{11.38}$$

$$\Delta P_{\text{op}} = I_{\text{MKS}} V_{\text{MKS}} \left\langle \frac{\Delta\gamma}{\gamma} \right\rangle, \tag{11.39}$$

where ΔP_{op} is now in watts. If the laser is oscillating in steady state, the power extracted from the electron beam on a single pass must leave the cavity on that pass, i.e. $\Delta P_{\text{op}} = P_{\text{out}}$. Thus, we have a quick way to calculate P_{out}, *if* we know the *extraction efficiency* $\langle \Delta\gamma/\gamma \rangle$. To obtain this, use the first of (11.9) for energy conservation,

$$2j_F \langle \Delta\nu \rangle_{\xi 0} = \Delta |a'|^2 = G_{\text{sat}} |a'|^2 \qquad \text{(in general)} \tag{11.40}$$

$$= \frac{G'}{4.36} (14.3)^2 \qquad \text{(optimum cavity loss; mnemonic).} \tag{11.41}$$

For optimum cavity losses we thus have, using mnemonic coefficients,

$$4\pi N_w \left\langle \frac{\Delta\gamma}{\gamma} \right\rangle = \langle \Delta\nu \rangle = 46.9 \frac{G'}{2j_F}, \tag{11.42}$$

$$\text{or} \quad \left\langle \frac{\Delta\gamma}{\gamma} \right\rangle = 1.866 \frac{G'}{j_F N_w}; \quad \left(\rightarrow \frac{1}{4N_w} \text{ as } j_F \rightarrow 0 \right). \tag{11.43}$$

As an illustration, in the previous example we had $j_F = 7.792$ and $G' = 1.355$, so $\langle \Delta\gamma/\gamma \rangle = \frac{0.3245}{N_w}$. The output power from (11.39) is $P_{\text{out}} = I_{\text{MKS}} V_{\text{MKS}} \langle \Delta\gamma/\gamma \rangle =$ (30 A)(42.511 MeV)(0.006904) = 8.80 MW, as calculated previously using mnemonic coefficients.

More generally, if j_F and δ_c are arbitrary, so that the cavity losses are not optimized, then the procedure for calculating the extraction efficiency is to find G_{sat} from (11.14) and $|a'|^2$ from (11.10). Then the decrease in phase velocity is $\langle \Delta\nu \rangle = G_{\text{sat}} |a'|^2 / 2j_F$, the extraction efficiency is $\langle \Delta\gamma/\gamma \rangle = \langle \Delta\nu \rangle / 4\pi N_w$, and the output power is $P_{\text{out}} = \eta_{\text{oc}} I_{\text{beam}} V_{\text{beam}} \langle \Delta\gamma/\gamma \rangle$.

The extraction efficiency is inversely proportional to the number of undulator periods N_w (11.43). Therefore, an FEL with fewer undulator periods will yield larger optical power at saturation (11.39), all other things being equal. Of course, the laser gain also decreases with fewer periods, so there is a trade-off in the design of the FEL. However, we do not have to change the design of the FEL to observe an

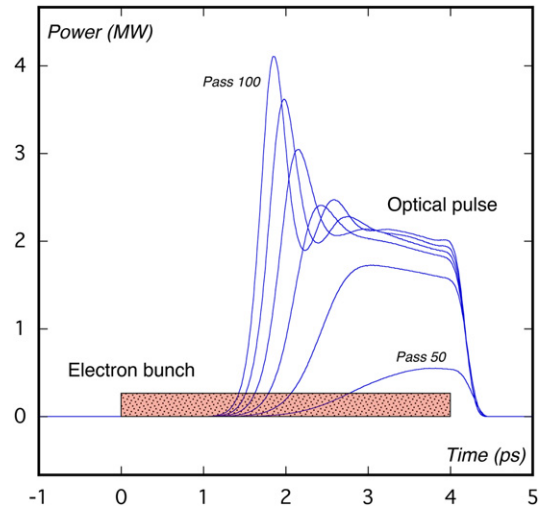

Figure 11.7. Numerical simulation of laser oscillation near the synchronous cavity length.

enhancement in extraction efficiency: there is an interesting phenomenon related to this effect that appears in numerical FEL pulse propagation simulations and provides a nice illustration of the physics involved.

Figure 11.7 is the result of a numerical simulation showing the formation of a saturated optical pulse at 3.2 μm in the Mark III FEL, operating near the synchronous cavity length. The FEL is driven by a train of rectangular electron bunches located between $t = 0$ ps and $t = 4$ ps in the numerical window, with the leading edge on the left. The figure shows the relative overlap between the two pulses at the start of the undulator at ten-pass intervals in the resonator. We see two interesting effects. First, by the time the optical pulse enters the large signal regime around pass 50, laser lethargy in the small signal regime has pushed the optical pulse towards the trailing edge of the electron bunch. The laser evidently saturates before the optical pulse walks off entirely, at which point lethargy is 'frozen' and the leading edge moves forward again under the combined action of the laser interaction and the finite (albeit small) cavity detuning. The second thing we observe is the abrupt formation of a narrow spike at the leading edge of the optical pulse with more than twice the peak power of the trailing section of the pulse.

What is the origin of this spike? The answer is the $1/N_w$ dependence of the FEL extraction efficiency. As the laser evolves more deeply into saturation, most of the electrons in the bunch (between ~1.5–4 ps on the latter passes) overlap and interact with the optical pulse for the entire length of the undulator, the full N_w periods. But the electrons at the leading edge of the bunch are not overlapped at all when the pulses first enter the undulator. Electrons positioned within one slippage length in advance of the sharp, leading edge of the optical pulse will not participate in the FEL interaction until the optical pulse slips past them some distance along the undulator. These electrons interact with the optical field over a reduced number of undulator periods $N_w^{\text{eff}} < N_w$. As a result, they experience greater extraction

efficiency, and dump their energy at the leading edge of the optical pulse in an increasingly tall and narrow spike roughly one slippage length wide. This spike often serves as a seed for the formation of sidebands: the smaller ripples following the leading spike in the optical pulse are actually the onset of the sideband instability.

11.6 Incorporation of energy spread

To include energy spread in the analysis of saturation, we perform a numerical integration of the CW coupled equations, (9.52) and (9.53),

$$\frac{\mathrm{d}a'}{\mathrm{d}\tau} = -j_F \langle \mathrm{e}^{-\mathrm{i}\xi'} \rangle_{\xi_0', \nu_0'} \tag{11.44}$$

$$\frac{\mathrm{d}\nu'}{\mathrm{d}\tau} = |a'| \cos(\xi' + \phi'), \tag{11.45}$$

but we include a second dimension in the initial phase space distribution to impose a normalized Gaussian energy spread in ν_0', (10.22), on the initially uniform distribution in phase ξ_0'. The same physical constraints—absence of frequency pulling, sideband formation, and short-pulse perturbations—are assumed to apply here as in section 11.3. For small optical fields, the small-signal gain obtained from the numerical integration of (11.44) and (11.45) agrees with the gain obtained from a numerical integration of the weak field solution, (10.27), with an accuracy of $|\Delta G|/G < 0.36\%$ over the full range $\sigma \leqslant 4$ and $j_F \leqslant 22$. Integration of the coupled equations for large optical fields satisfies energy conservation to within roughly twice this error.

To achieve useful approximations to the solution for large optical fields over the full range of σ and j_F, we first derive an improved approximation to the inhomogeneous gain reduction factor q_γ in the calculation of the small-signal gain, (10.28). The revised calculation allows the two numerical coefficients in (10.24) to include a dependence on j_F, yielding a new gain reduction factor q_γ' given by

$$q_\gamma' \simeq \frac{1}{\left[1 + \left(\dfrac{\sigma}{A(j_F)}\right)^2\right]^{B(j_F)}}, \tag{11.46}$$

where

$$A(j_F) = 3.27 + 0.0183\, j_F - 0.000169\, j_F^2 \tag{11.47}$$

$$B(j_F) = 1.80 + 0.0138\, j_F - 0.000160\, j_F^2 . \tag{11.48}$$

The use of this gain reduction factor in the calculation of the small-signal gain,

$$G_\gamma' = G'(j_F\, q_\gamma'), \tag{11.49}$$

where $G'(...)$ is the three-term expansion defined by (10.15), yields an accuracy of $|\Delta G'_\gamma|/G'_\gamma < 1\%$ for $\sigma \leqslant 4$ and $j_F \leqslant 22$.

The intensity dependence of the saturated gain G_{sat} in the presence of energy spread is then obtained by fitting each of the coefficients '4π' and '$\sqrt{\pi}$' in (11.10) to a series expansion in products $j_F^n \sigma^m$. Upon solving (11.44) and (11.45) numerically at peak ${\nu_0'}^{\text{opt}}$, we can approximate the results by the following expression:

$$G'_{\text{sat}} \equiv \frac{\Delta|a'|^2}{|a'|^2} = \frac{G'_\gamma}{\left[1 + \left(\dfrac{|a'|}{\alpha_\gamma}\right)^2\right]^{\beta_\gamma}}, \tag{11.50}$$

where the parameters α_γ and β_γ are given by the power series expansions

$$\alpha_\gamma = \sum_{n=0}^{3}\sum_{m=0}^{4} \alpha_{nm} j_F^n \sigma^m; \quad \beta_\gamma = \sum_{n=0}^{3}\sum_{m=0}^{4} \beta_{nm} j_F^n \sigma^m, \tag{11.51}$$

and the numerical coefficients α_{nm} and β_{nm} are the corresponding elements of the following coefficient matrices:

$$\alpha_{nm} = \begin{pmatrix} 13.60 & -0.277 & 2.09 & -0.367 & 0.0198 \\ -0.257 & 0.00833 & -0.0465 & 0.0170 & -0.00164 \\ 0.00942 & 0.000107 & 0.000272 & -0.000307 & 0.0000409 \\ -0.000150 & -3.31\times10^{-6} & 5.87\times10^{-6} & 2.08\times10^{-6} & -4.44\times10^{-7} \end{pmatrix}, \tag{11.52}$$

$$\beta_{nm} = \begin{pmatrix} 1.800 & -0.0287 & 0.177 & -0.0463 & 0.00352 \\ -0.0114 & 0.00150 & -0.00924 & 0.00330 & -0.000321 \\ 0.000864 & -0.0000115 & 0.000157 & -0.0000798 & 9.13\times10^{-6} \\ -0.0000159 & 8.44\times10^{-8} & -1.36\times10^{-6} & 1.02\times10^{-6} & -1.32\times10^{-7} \end{pmatrix}. \tag{11.53}$$

For $\sigma \leqslant 4$ and $j_F \leqslant 22$ these coefficients convey an accuracy of $|\Delta G'_{\text{sat}}|/G'_{\text{sat}} < 3.5\%(8\%)$ for $|a'| \leqslant 18(29)$.

Numerical values for G'_γ, α_γ and β_γ obtained from the above expressions can be used directly in the analysis of optical resonators developed in section 11.4. For example, the optimum intracavity power, saturated gain, cavity loss and output power from (11.19)–(11.22) are

$$|a'|^2_{\text{opt}} = \frac{(\alpha_\gamma)^2}{\beta_\gamma - 1}; \quad G'_{\text{sat}} = \frac{G'_\gamma}{\left[1 + \dfrac{1}{\beta_\gamma - 1}\right]^{\beta_\gamma}}; \quad \delta_c^{\text{opt}} = \frac{G'_{\text{sat}}}{1 + G'_{\text{sat}}}; \quad |a'|^2_{\text{out}} = |a'|^2_{\text{opt}} G'_{\text{sat}} \eta_{\text{oc}}. \tag{11.54}$$

The application of these results will be illustrated in section 12.2, where the effects of energy spread are of particular significance for lasing on higher harmonics.

Numerical approximations notwithstanding, the above analysis reveals some interesting physics about the effects of energy spread on the saturation mechanism in FELs. First, examine the dependence of the coefficients α_γ and β_γ on the energy spread σ. These dependencies are plotted in figure 11.8.

The coefficient β_γ increases only slightly with energy spread, from ~1.8 to 2.4 over the range of σ shown, but the coefficient α_γ roughly doubles over the same range. Since α_γ^2 plays the role of a 'saturation intensity', the increase in α_γ with energy spread leads to larger saturated powers than would otherwise ensue if α_γ and β_γ were independent of σ. This behavior counteracts the detrimental effect of inhomogeneous gain reduction in the small-signal regime. The corresponding effect on the output power $|a'|^2_{\text{out}}$ is illustrated in figure 11.9 for a current of $j_F = 8$. These curves

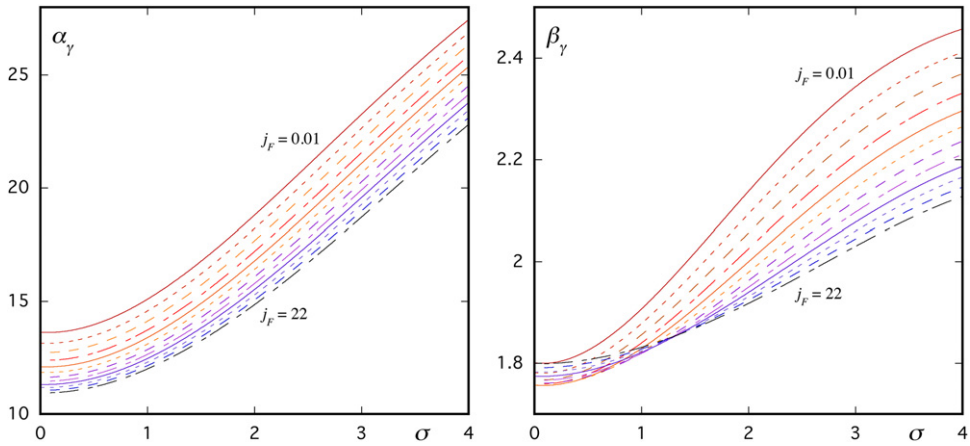

Figure 11.8. FEL saturation coefficients α_γ and β_γ versus energy spread σ; $j_F = 0.01, 2, 4, 6, \ldots, 22$.

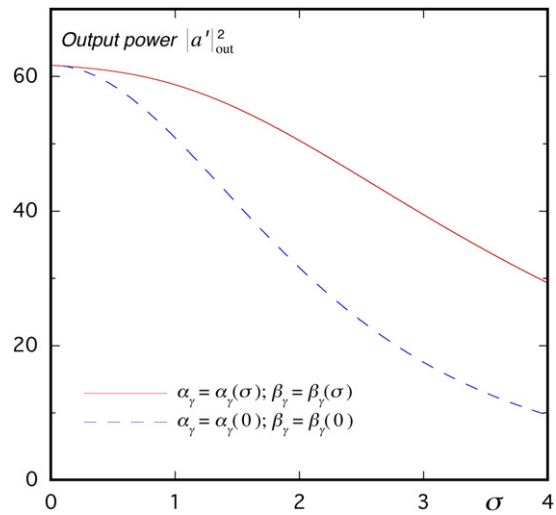

Figure 11.9. Optimum output power versus energy spread at saturation; $j_F = 8$; $\eta_{\text{oc}} = 1$.

show the optimum output power calculated from (11.54) assuming the full variation of G_γ' with energy spread according to (11.49)—but the dashed curve is the optimum output power calculated with constant coefficients $\alpha_\gamma(\sigma = 0); \beta_\gamma(\sigma = 0)$, while the solid curve assumes the full σ-dependence $\alpha_\gamma(\sigma); \beta_\gamma(\sigma)$ given by (11.51). We see that the σ-dependence of the coefficients yields a significant increase in power at all values of the energy spread. Equation (11.54) reveals that the optimum output power $|a'|^2_{\text{out}}$ with fixed coefficients is strictly proportional to the small-signal gain G_γ', i.e. the output power is afflicted by the full effect of inhomogeneous gain reduction. The enhancement of output power that actually occurs for variable coefficients motivates the aphorism that 'the FEL interaction is more accommodating of energy spreads at saturation'.

The energy acceptance of the FEL can be equivalently defined in both the small signal and large signal regimes. In the small signal regime, the form of the small signal gain curve requires that the $1/e$ energy half-width satisfy $\Delta\nu_0 \leqslant 2.6$, so that all the electrons contribute a positive gain. In the optimized FEL interaction at saturation, the behavior of the electron orbits in phase space similarly requires $\Delta\nu_0 \leqslant 2.6$, so that all the electrons undergo half a phase space revolution in the *downward* direction. Since $\Delta\nu_0 = \sqrt{2}\,\sigma$, we require in either case that $\sigma \lesssim 2.6/\sqrt{2} \simeq 2$, or $(\delta\gamma/\gamma)_{1/e} \lesssim 1/2N_w$ (10.25). This is the *energy acceptance* of the FEL and yields a fundamental constraint on the quality of the energy spread in the electron beam.